ACS OMEGA

Open Access

http://pubs.acs.org/journal/acsodf

Article

Exploring the Anti-Inflammatory Effect of Tryptanthrin by Regulating TLR4/MyD88/ROS/NF-κB, JAK/STAT3, and Keap1/Nrf2 Signaling Pathways

Jie Zhu, Wen Cheng, Tian-Tian He, Bao-Long Hou, Li-Yan Lei, Zheng Wang,* and Yan-Ni Liang*

Cite This: *ACS Omega* 2024, 9, 30904−30918

Read Online

ACCESS | Metrics & More | Article Recommendations

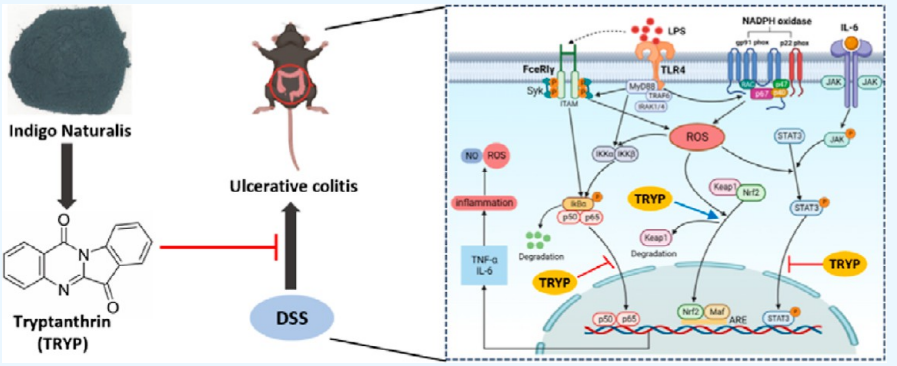

ABSTRACT: Tryptanthrin (TRYP) is the main active ingredient in Indigo Naturalis. Studies have shown that TRYP had excellent anti-inflammatory activity, but its specific mechanism has been unclear. In this work, the differentially expressed proteins resulting from TRYP intervention in LPS-stimulated RAW264.7 cells were obtained based on tandem mass tag proteomics technology. The anti-inflammatory mechanism of TRYP was further validated by a combination of experiments using the LPS-induced RAW264.7 cell model in vitro and the DSS-induced UC mouse model (free drinking 2.5% DSS) in vivo. The results demonstrated that TRYP could inhibit levels of NO, IL-6, and TNF-α in LPS-induced RAW264.7 cells. Twelve differential proteins were screened out. And the results indicated that TRYP could inhibit upregulated levels of gp91phox, p22phox, FcεRIγ, IKKα/β, and p-IκBα and reduce ROS levels in vitro. Besides, after TRYP treatment, the health conditions of colitis mice were all improved. Furthermore, TRYP inhibited the activation of JAK/STAT3, nuclear translocation of NF-κB p65, and promoted the nuclear expression of Nrf2 in vitro and in vivo. This work preliminarily indicated that TRYP might suppress the TLR4/MyD88/ROS/NF-κB and JAK/STAT3 signaling pathways to exert anti-inflammatory effects. Additionally, TRYP could achieve antioxidant effects by regulating the Keap1/Nrf2 signaling pathway.

1. INTRODUCTION

Inflammation plays a crucial role in the body's defense against pathogens.[1] Macrophages are important in the initiation and regulation of host defenses and can be activated by diverse inflammatory stimuli, such as lipopolysaccharides (LPS), to trigger a cascade of inflammatory processes.[2] In RAW264.7, the toll-like receptor (TLR4) activates the corresponding signaling pathway by binding to the ligand LPS, which induces several active factors and leads to immune responses, such as inflammation. TLR4 activation promotes the production of reactive oxygen species (ROS) and inflammatory factors.[3] Generally, the NF-κB dimers are sequestered by NF-κB (IκBs) inhibitors, however, under-stimulated with LPS, activated inhibitor of kappa B kinase (IKK) can phosphorylate IκBs, leading to NF-κB nuclear translocation.[4] Janus kinase/signal transducer and activator of transcription (JAK/STAT) can promote inflammatory responses by regulating a variety of signals.[5] Upon binding to its receptor, IL-6 activates downstream JAKs, leading to STAT3 phosphorylation. Subsequently, p-STAT3 enters the nucleus and binds to specific target gene sites and regulates gene expression.[4,6−9]

Ulcerative colitis (UC) is a chronic inflammatory disease that commonly presents with symptoms such as abdominal pain and bloody stools.[10] Defective gut epithelial barrier, alteration of intestinal flora, and dysregulated immune

Received: April 20, 2024
Revised: June 21, 2024
Accepted: June 24, 2024
Published: July 3, 2024

responses are all associated with the incidence of UC. The inflammatory pathology of UC is significant, such as the diffuse inflammatory infiltration in colonic mucosa, the increase of lymphocytes and plasma cells in the lamina propria. Although the role of macrophages in colitis is unknown, disorders of monocytes and macrophages occur in intestinal inflammation.[11,12] In addition, the release and imbalance of inflammatory cytokines promoted the occurrence and development of colitis. These factors interact with each other and mediate intestinal homeostasis, ultimately influencing the course of UC.[13] The dextran sulfate sodium (DSS)-induced UC model synthesizes and releases large amounts of pro-inflammatory cytokines (such as TNF-α and IL-6) and activates multiple inflammatory signaling pathways, which has been a classic model for studying the effects of colitis drugs.

Indigo Naturalis (IN) (also called Qingdai; Figure 1A) is a traditional Chinese medicine. It is a dry powder processed from the leaves or stems of blue-producing plants, including *Baphicacanthus cusia* (Nees) Bremek, *Polygonum tinctorium* W.T.Aiton, and *Isatis indigotica* Fortune. Pharmacological studies have shown that IN had antipyretic,[14] antibacterial,[15] anti-inflammatory, and other pharmacological effects.[16] Due to its excellent anti-inflammatory effects, IN is clinically used to treat UC,[17] acute promyelocytic leukemia, and psoriasis.[18,19] The active ingredients of IN are mainly indigo, indirubin, and tryptanthrin (indolo[2,1-*b*]quinoline-6,12-dione, TRYP) (Figure 1B). Multiple studies have shown that indigo, indirubin, and TRYP exhibited excellent anti-inflammatory activities.[20−22] Our previous study also found that TRYP exerted an anti-inflammatory effect on UC mice by modulating the secretion of inflammatory factors and decreasing the expression of NF-κB p65 in mouse colon tissues.[23,24] In addition, it has been reported that TRYP could reduce the production of inflammatory factors in BV2 cells by regulating the Nrf2/HO-1 and NF-κB signaling pathways.[25]

Overall, TRYP has significant anti-inflammatory activity even in UC mice, but its exact mechanism of action is still unclear. Exploring the anti-inflammatory mechanism of TRYP is helpful for its redevelopment and utilization. In this study, the inflammation model in RAW264.7 cells was induced with LPS, and the tandem mass spectrometry (TMT)-proteomics was used to identify the differential proteins regulated by TRYP. Based on the TMT results, the related pathways were analyzed, evaluated, and verified by in vitro experiments. The DSS-induced UC mouse model was adopted to validate the key targets of the relevant pathway, further elucidating the anti-inflammatory mechanism of TRYP.

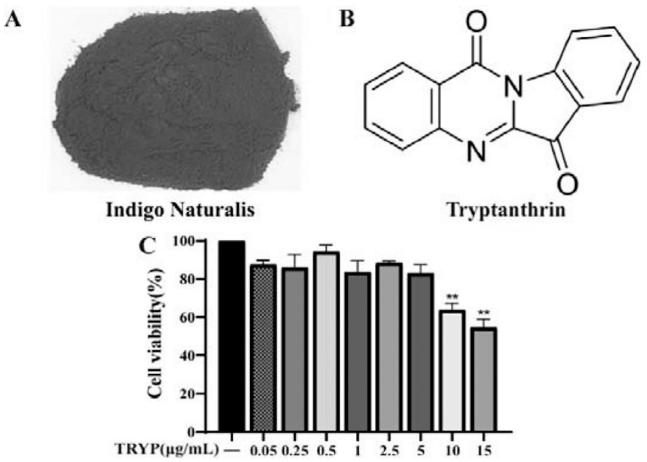

Figure 1. (A) Indigo Naturalis. (B) TRYP structure. (C) Effect of TRYP on RAW264.7 macrophage viability (%). $^{**}P < 0.01$ vs control group.

2. RESULTS

2.1. Cell Viability. The effect of TRYP on the survival rate of RAW264.7 cells was detected by the MTT assay. The results indicated that TRYP had no significant inhibitory effect on RAW264.7 cells below 10 μg/mL (Figure 1C); therefore, 1, 2.5, and 5 μg/mL were selected as the final TRYP concentrations.

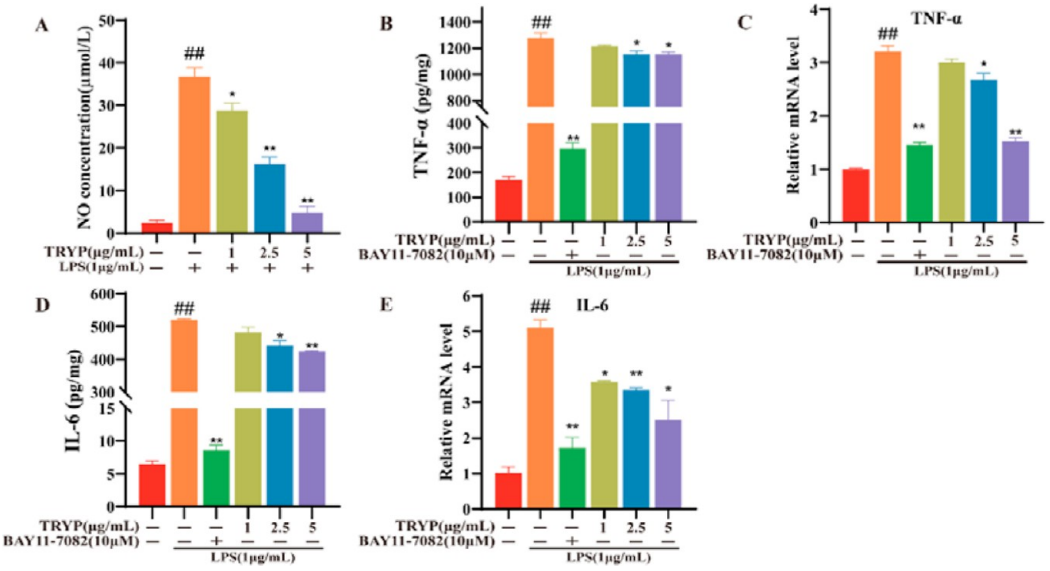

Figure 2. Effect of TRYP on the expression levels of inflammatory factors. The relative secretion and mRNA expression of NO (A), TNF-α (B,C), and IL-6 (D,E). $^{\#\#}P < 0.01$ vs control group; $^{*}P < 0.05$, $^{**}P < 0.01$ vs LPS group.

https://doi.org/10.1021/acsomega.4c03795
ACS Omega 2024, 9, 30904−30918

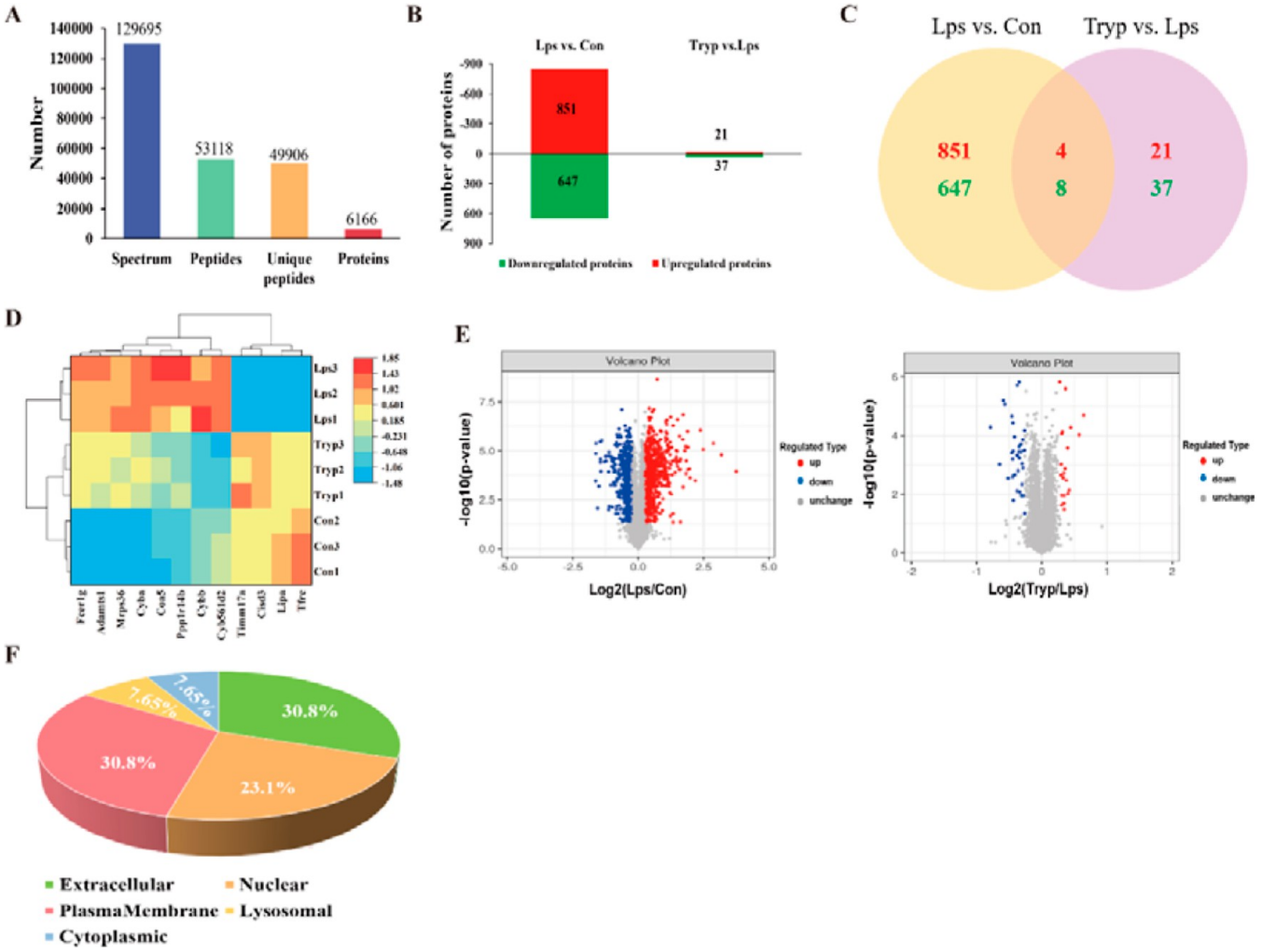

Figure 3. Quantitative analysis results for TMT proteomics. (A) Protein identification and quantitative results. (B) Number of upregulated and downregulated proteins between groups. (C) Venn diagram. Red represents upregulated, and green represents downregulated. (D) Cluster analysis of 12 differentially expressed proteins. (E) Significantly different volcano plots for proteins in each group. (F) Subcellular localization of differentially expressed proteins.

Table 1. Information of 12 Differentially Expressed Proteins between Two Groups

			Lps/Con		Tryp/Lps	
accession	gene name	protein name	*P* value	variation trend	*P* value	variation trend
P20491	Fcer1g	high affinity immunoglobulin epsilon receptor subunit gamma	8.57×10^{-5}	↑	0.007643	↓
Q9CQX8	Mrps36	28S ribosomal protein S36, mitochondrial	4.92×10^{-5}	↑	0.010910	↓
Q61462	CYBA	cytochrome *b*-245 light chain	1.3×10^{-6}	↑	0.000343	↓
P97857	Adamts1	a disintegrin and metalloproteinase with thrombospondin motifs 1	4.43×10^{-7}	↑	0.000319	↓
Q99M07	Coa5	cytochrome c oxidase assembly factor 5	0.001071	↑	0.002524	↓
Q62084	Ppp1r14b	protein phosphatase 1 regulatory subunit 14B	0.005506	↑	0.016533	↓
Q61093	CYBB	cytochrome b-245 heavy chain	0.001072	↑	0.000503	↓
Q9WUE3	Cyb561d2	cytochrome b561 domain-containing protein 2	0.000202	↑	2.22×10^{-5}	↓
Q9Z0 V8	Timm17a	mitochondrial import inner membrane translocase subunit Tim17-A	1.14×10^{-5}	↓	0.001977	↑
Q9Z0M5	Lipa	lysosomal acid lipase/cholesteryl ester hydrolase	0.000168	↓	8.68×10^{-5}	↑
B1AR13	Cisd3	CDGSH iron−sulfur domain-containing protein 3, mitochondrial	0.000384	↓	5.34×10^{-5}	↑
Q62351	Tfrc	transferrin receptor protein 1	1.85×10^{-5}	↓	7.56×10^{-5}	↑

2.2. Effect of TRYP on the Expression Levels of Inflammatory Factors. NO secretion was significantly elevated in the LPS group compared with the control group (Figure 2A). NO secretion decreased significantly post TRYP treatment. As depicted in Figure 2B−E, LPS significantly elevated the expression levels of IL-6 and TNF-α which were significantly reduced in the TRYP (2.5, 5 μg/mL) and BAY11−7082 groups.

2.3. Proteomics Results and Verification. *2.3.1. Identification of Proteins and Statistical Results of Differential*

https://doi.org/10.1021/acsomega.4c03795
ACS Omega 2024, 9, 30904−30918

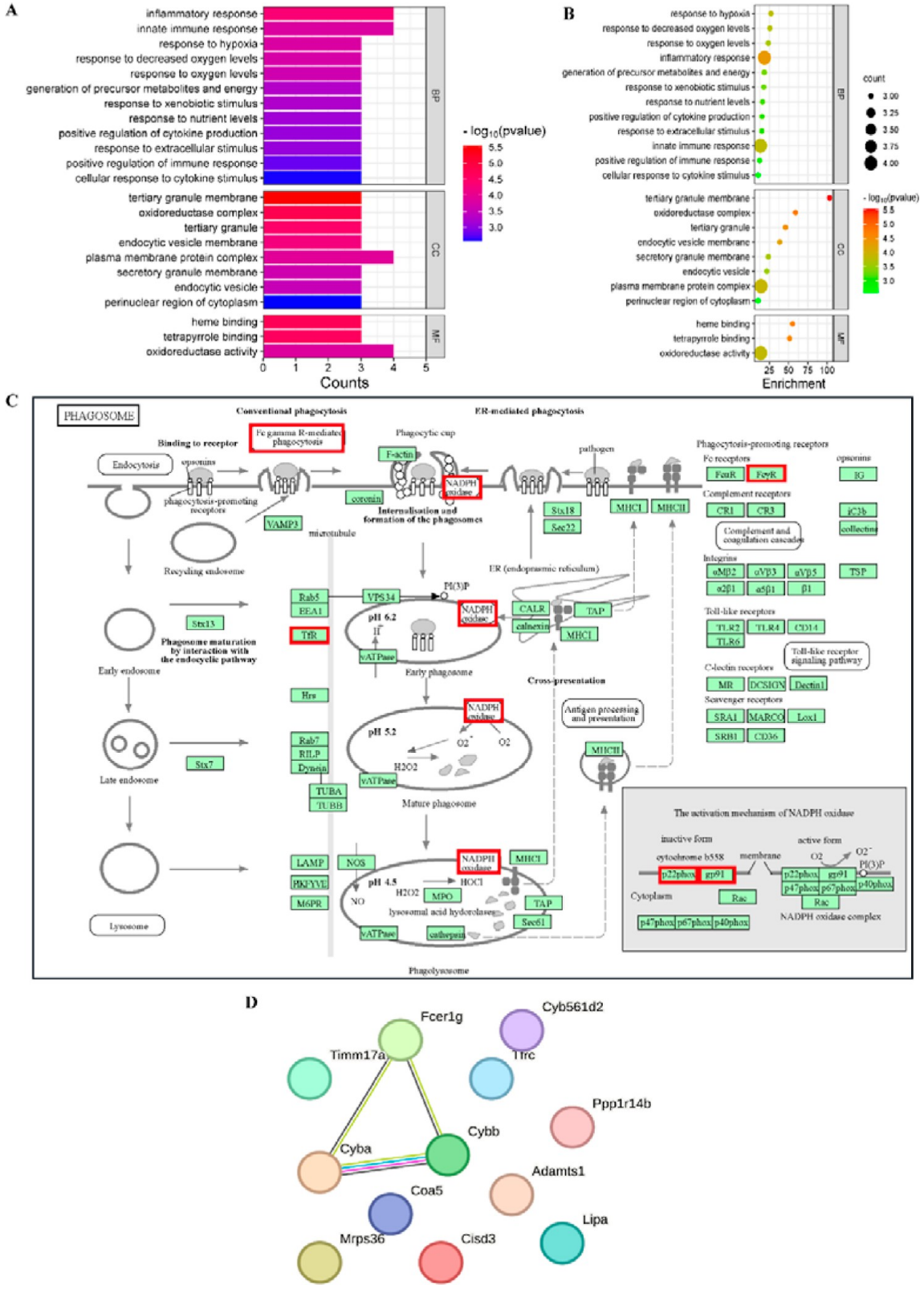

Figure 4. Results of GO, KEGG, and PPI analyses of differentially expressed proteins. (A) GO enrichment analysis histogram. (B) GO enrichment analysis bubble diagram. (C) KEGG signaling pathway of the phagosome. The red box is a differentially expressed protein involved in phagosome. (D) PPI network diagram of differentially expressed proteins.

Proteins. A total of 129,695 secondary mass spectra and 53,118 peptides were obtained using tandem mass spectrometry and quantitative TMT detection. 6166 proteins were identified from 49906 unique peptides (Figure 3A). Figure 3B shows that there were 25 proteins with increased expression and 45 proteins with decreased expression post TRYP treatment. Twelve differentially expressed proteins (Table 1) were present, including four upregulated and eight down-

https://doi.org/10.1021/acsomega.4c03795
ACS Omega 2024, 9, 30904−30918

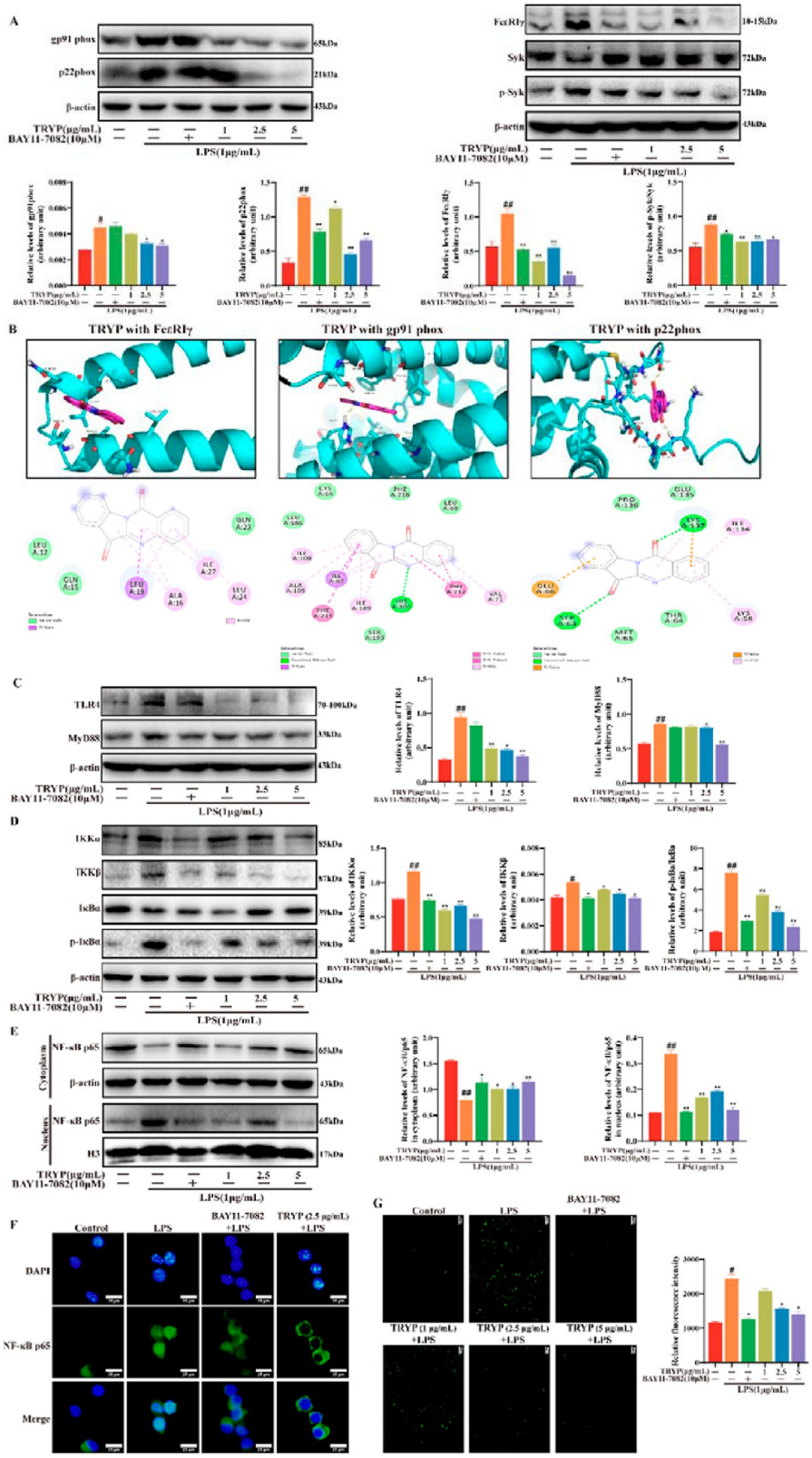

Figure 5. TRYP inhibited the TLR4/MyD88/ROS/NF-κB signaling pathway. (A) Expression levels of FcεRIγ, gp91phox, p22phox, Syk, and p-Syk. (B) Molecular docking. The binding modes of TRYP with FcεRIγ, TRYP with gp91phox, and TRYP with p22phox. The expression levels TLR4 and MyD88 (C), IKKα, IKKβ, IκBα, and p-IκBα (D), and NF-κB p65 (E). (F) Subcellular localization of the NF-κB p65 protein in each group. Scale bar = 25 μm. (G) ROS levels in each group. Scale bar = 100 μm. $^{\#\#}P < 0.01$, $^{\#}P < 0.05$ vs control group; $^{*}P < 0.05$, $^{**}P < 0.01$ vs LPS group.

regulated proteins (Figure 3C). Differentially expressed proteins were grouped and categorized using a hierarchical cluster algorithm and presented as a heatmap (Figure 3D). The variability in proteins between groups was demonstrated

https://doi.org/10.1021/acsomega.4c03795
ACS Omega 2024, 9, 30904−30918

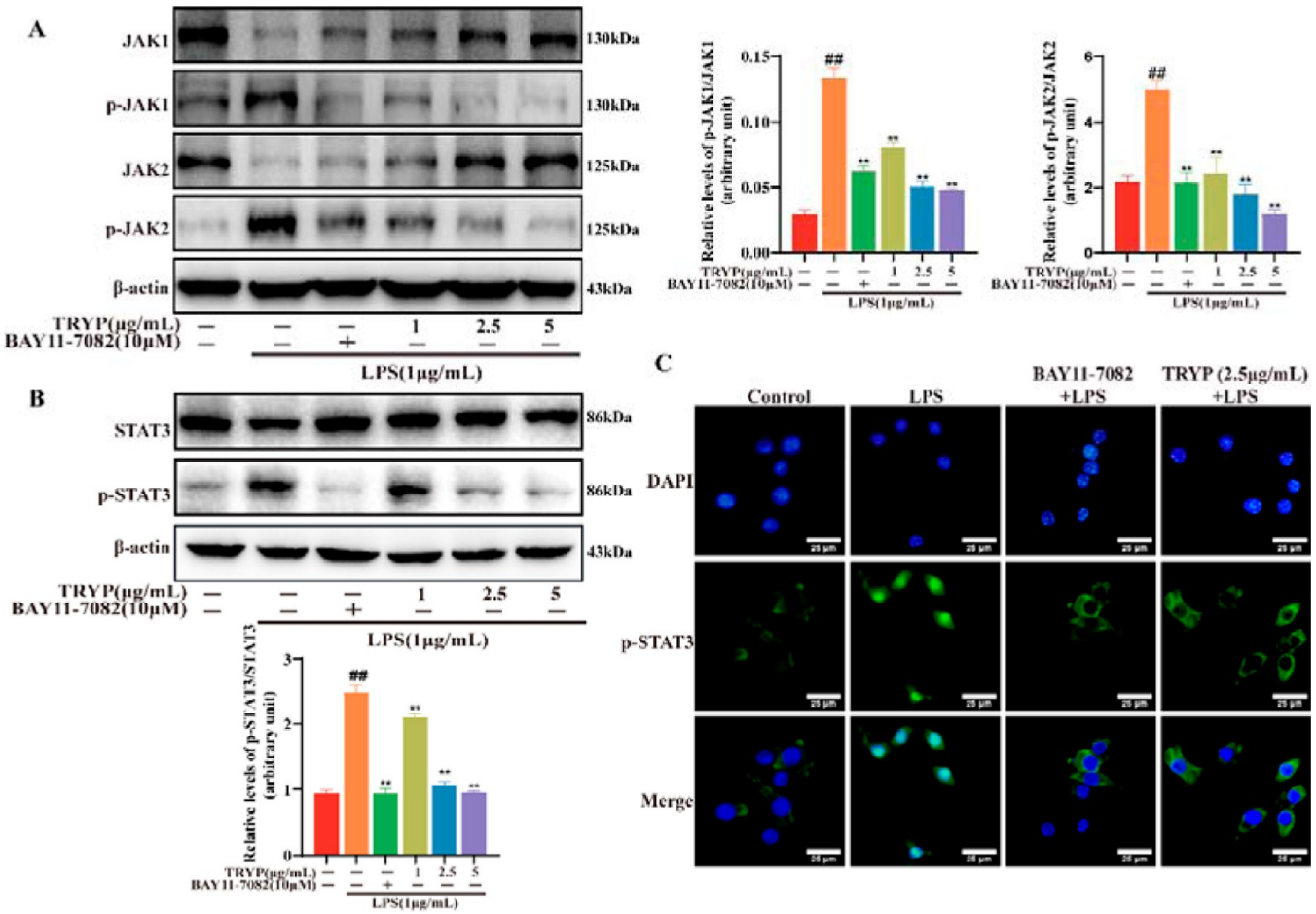

Figure 6. TRYP inhibited the JAK/STAT3 signaling pathway. (A,B) Expression levels of STAT3, p-STAT3, JAK1, *p*-JAK1, JAK2, and *p*-JAK2 proteins in each group. (C) Subcellular localization of the p-STAT3 protein in each group. Scale bar = 25 μm. $^{\#\#}P < 0.01$ vs control group; $^{**}P < 0.01$ vs LPS group.

by volcano plots, which were plotted in terms of FC and *P* values (*t*-test) (Figure 3E). The differentially expressed proteins were predominantly localized in the plasma membrane (30.8%), extracellular (30.8%), nucleus (23.1%), cytoplasm (7.65%), and lysosomes (7.65%) (Figure 3F).

2.3.2. Functional Enrichment of Differential Proteins. GO annotation was conducted on 12 differentially expressed proteins to understand their localization, function, and biological pathways involved in the organism. GO enrichment analysis revealed eight enrichment items for cellular components, three enrichment items for molecular functions, and 12 enrichment items for biological processes (Figure 4A,B). Differentially expressed proteins were predominantly involved in cellular components, such as plasma membranes; molecular functions, such as oxidoreductase activity; and biological processes, such as inflammatory responses. KEGG pathway enrichment analysis obtained a pathway, the phagosome pathway (Figure 4C).

2.3.3. PPI Network Analysis. The disconnected nodes of the PPI network were hidden, and finally, three nodes and three edges were obtained. Among the differentially expressed proteins, gp91phox (encoded by CYBB), p22phox (encoded by CYBA), and FcεRIγ (encoded by Fcer1g) were related to each other (Figure 4D). gp91phox and p22phox are the key NADPH oxidase subunits.[26] FcεRIγ is the gamma chain of the immunoglobulin ε receptor, and FcεRIγ has immunoreceptor tyrosine-based activation motifs (ITAMs) essential for signaling.[27]

Through our analysis, we speculated that the mechanism of action of TRYP on LPS-induced RAW264.7 cells might involve the TLR4/MyD88/ROS/NF-κB, JAK/STAT3, and Keap1/Nrf2 signaling pathways. Next, our speculation was preliminarily verified by relevant experiments.

2.3.4. TRYP Inhibited the TLR4/MyD88/ROS/NF-κB Signaling Pathway. Three proteins, gp91phox, p22phox, FcεRIγ and p-Syk, were lowly expressed in the control group and were significantly upregulated post LPS stimulation, while TRYP could significantly downregulate their expression. BAY11-7082 (10 μM) had negligible inhibitory effect on gp91phox. p22phox protein expression, however, could inhibit FcεRIγ protein expression (Figure 5A). As gp91phox, p22phox, and FcεRIγ are located on the cell membrane, we speculated that TRYP may bind to them. Based on this hypothesis, we conducted molecular docking experiments. The results demonstrated the binding energies of FcεRIγ, gp91phox, and p22phox with TRYP of −6.0, −9.9, and −6.4 kcal/mol, respectively (Figure 5B). TRYP exhibits strong binding activity with gp91phox, p22phox, and FcεRIγ.

Our results demonstrated that TLR4 and MyD88 expression increased after LPS stimulation and decreased in the TRYP group (Figure 5C). BAY11-7082 (10 μM) had negligible effect on TLR4 and MyD88 protein expression. The expression of p-

https://doi.org/10.1021/acsomega.4c03795
ACS Omega 2024, 9, 30904−30918

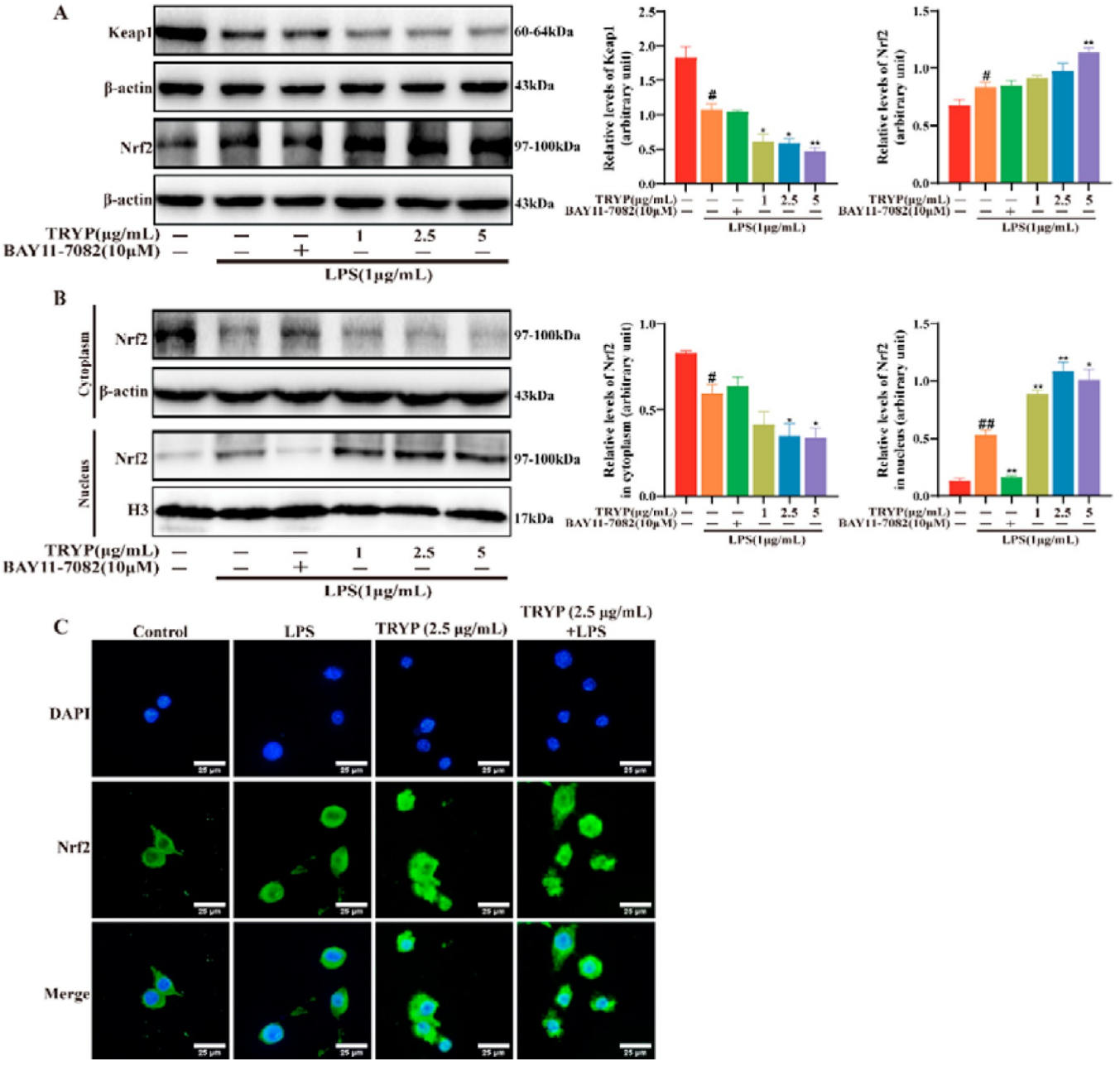

Figure 7. Regulatory effect of TRYP on the Keap1/Nrf2 signaling pathway. Western blotting analysis of Keap1 and Nrf2 (A) and Nrf2 in the cytoplasm and nucleus (B). (C) Subcellular localization of the Nrf2 protein in each group. Scale bar = 25 μm. $^{\#\#}P < 0.01$, $^{\#}P < 0.05$ vs the control group; $^{*}P < 0.05$, $^{**}P < 0.01$ vs the LPS group.

IκBα, IKKα, IKKβ, and NF-κB p65 (in nucleus) increased post LPS stimulation. However, TRYP and BAY11-7082 pretreatment reduced their expression (Figure 5D,E). Immunofluorescence (IF) experiments also displayed stronger green fluorescence in the LPS group and weaker fluorescence in the TRYP and BAY11-7082 groups, suggesting that TRYP could inhibit the transfer of NF-κB p65 to the nucleus (Figure 5F).

ROS can induce IκB protein modification, thereby activating NF-κB.[28] The results demonstrated that green fluorescence was significantly enhanced post LPS stimulation, indicating a dramatic increase in ROS levels. Conversely, the TYRP treatment significantly suppressed ROS levels. The ROS levels also decreased post BAY11-7082 treatment (Figure 5G). These results indicated that TRYP had a protective effect on LPS-induced RAW264.7 cells and could reduce the ROS levels.

2.3.5. TRYP Inhibited the JAK/STAT3 Signaling Pathway. The phosphorylation level of STAT3 significantly increased after LPS stimulation. Conversely, TRYP pretreatment could reduce the STAT3 phosphorylation level. The expression of phosphorylated JAK1 and JAK2 was upregulated post LPS stimulation and significantly downregulated in the TRYP pretreatment group in a dose-dependent manner (Figure 6A,B). BAY11-7082 treatment significantly reduced the levels of p-STAT3, p-JAK1, and p-JAK2 expression. As depicted in Figure 6C, p-STAT3 was highly expressed post LPS stimulation, and most of them were localized in the nucleus. Conversely, TRYP and BAY11-7082 significantly inhibited the entry of p-STAT3 into the nucleus. These studies demon-

https://doi.org/10.1021/acsomega.4c03795
ACS Omega 2024, 9, 30904−30918

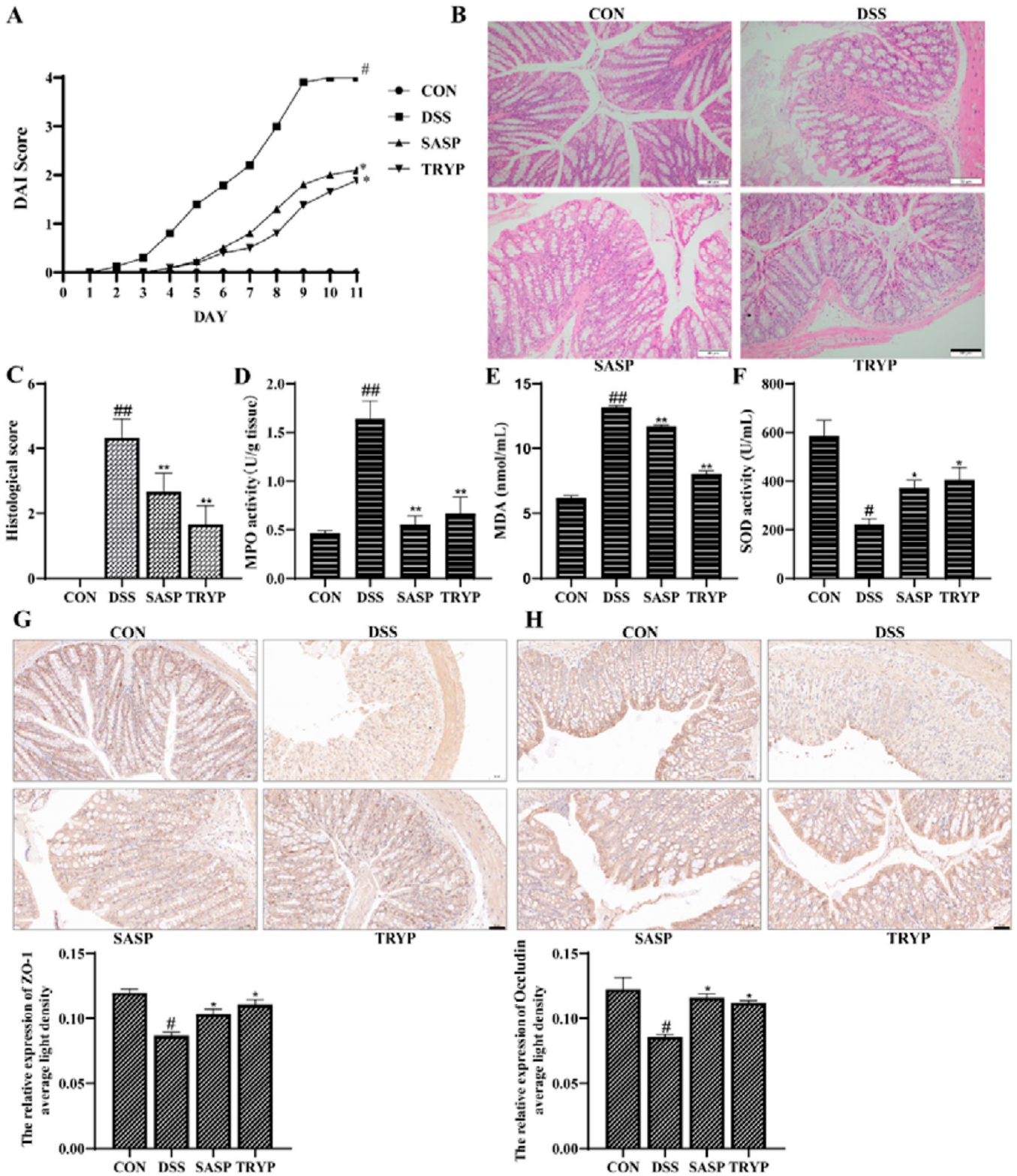

Figure 8. Effect of TRYP on UC mice. (A) DAI score. (B,C) Pathological section and scoring of colon tissue. (D) MPO activity. (E) Levels of MDA. (F) SOD activity. Immunohistochemistry and quantification of ZO-1 (G) and occludin (H). Images were acquired at 20×, scale bar 50 μm. $^{\#\#}P < 0.01$, $^{\#}P < 0.05$ vs CON group; $^{*}P < 0.05$, $^{**}P < 0.01$ vs DSS group.

strated that TRYP pretreatment inhibited the activation of the JAK/STAT3 signaling pathway.

2.3.6. Regulatory Effect of TRYP on the Keap1/Nrf2 Signaling Pathway. The Keap1/Nrf2 pathway is a crucial cellular defense mechanism against oxidative stress injury.[29] The results depicted in Figure 7A indicate that LPS stimulation caused a decrease in Keap1 protein expression, which was even more reduced in the TRYP-pretreated group. Compared with the LPS group, BAY11-7082 treatment had negligible effect on Keap1 protein expression. LPS stimulation could activate Nrf2

https://doi.org/10.1021/acsomega.4c03795
ACS Omega 2024, 9, 30904−30918

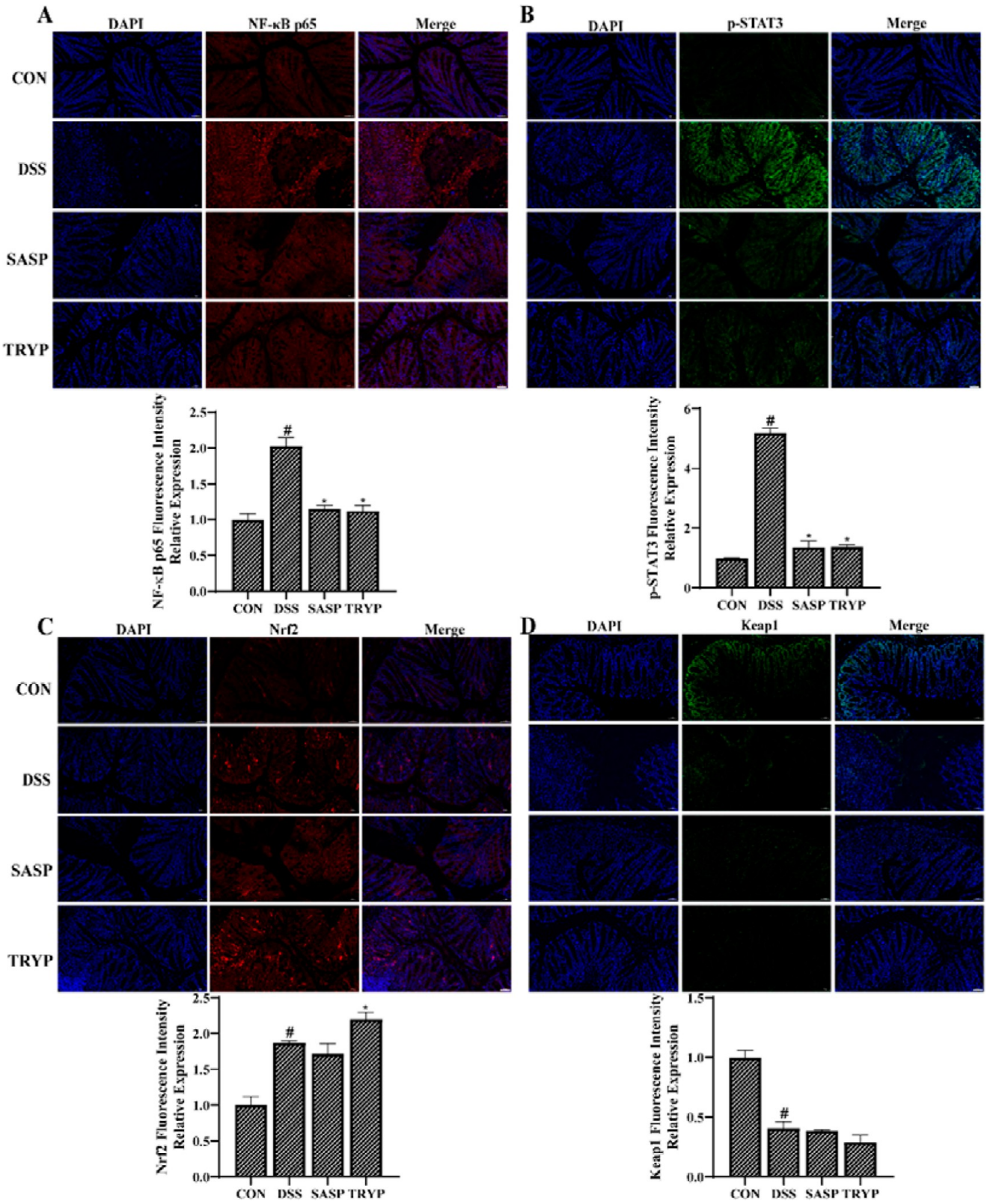

Figure 9. Mechanism of TRYP in the treatment of UC mice. IF and quantification of NF-κB p65 (A), p-STAT3 (B), Nrf2 (C), and Keap1 (D). Images were acquired at 20×, scale bar 50 μm. $^{\#}P < 0.05$ vs CON group; $^{*}P < 0.05$ vs DSS group.

and promote its entry into the nucleus. TRYP pretreatment could increase Nrf2 expression and further activated Nrf2 signaling (Figure 7B). IF results (Figure 7C) demonstrated that the fluorescence intensity of Nrf2 increased post LPS stimulation. Compared with the LPS group, Nrf2 was highly expressed in the nucleus and cytoplasm in the TRYP treatment and the TRYP pretreatment groups.

2.4. Effect of TRYP on UC Mice. *2.4.1. Disease Activity Index Score and Colon Pathology.* The results in Figure 8A showed that 2.5% DSS could induce colitis successfully. After

https://doi.org/10.1021/acsomega.4c03795
ACS Omega 2024, 9, 30904−30918

administration of salazosulfapyridine (SASP) and TRYP, the disease activity index (DAI) score was decreased, intestinal inflammatory damage was improved, and inflammatory infiltration was reduced (Figure 8A−C). Moreover, DSS-induced MPO activity in the colon of mice was significantly increased, which was significantly decreased after TRYP treatment (Figure 8D). The above results showed that the TRYP treatment effectively reduced colon inflammation in UC mice.

2.4.2. Effect of TRYP on Oxidative Stress in UC Mice. Oxidative stress is an important mechanism for the development of UC. After DSS induction, the content of MDA in mice was significantly increased, while the activity of SOD was significantly decreased, indicating that DSS modeling increased the level of oxidative stress in mice. Compared with the DSS group, the content of MDA in the SASP group and TRYP group was downregulated, while the activity of SOD was upregulated significantly, suggesting that TRYP treatment could inhibit the oxidative stress level of DSS-induced UC mice (Figure 8E,F).

2.4.3. Effect of TRYP on Intestinal Tight Junction Proteins in UC Mice. The characteristics of UC also include decreased expression of intestinal tight junction proteins (such as ZO-1 and occludin), leading to increased permeability of the intestinal mucosa. The expression levels of occludin and ZO-1 proteins in the DSS group were significantly downregulated, indicating a significant increase in intestinal permeability. With treatment of SASP and TRYP, the expression of ZO-1 and occludin was all increased, respectively (Figure 8G,H). The above showed that TRYP could protect against DSS-induced colitis by regulating tight junction proteins to reduce intestinal permeability.

2.4.4. Effect of TRYP on NF-κB/STAT3 and Keap1/Nrf2 Signaling Pathways in UC Mice. The effects of TRYP on NF-κB/STAT3 and Keap1/Nrf2 signaling pathways were verified in vivo by the IF assay. The phosphorylation levels of STAT3 and nuclear translocation of NF-κB p65 were all significantly increased in colitis. After treatment with SASP and TRYP, the levels of NF-κB p65 in the nucleus and p-STAT3 were all sharply decreased (Figure 9A,B). These results indicated that TRYP could suppress the activation and translocation of NF-κB p65 and p-STAT3.

The expression of Nrf2 was notably upregulated and that of Keap1 was dramatically downregulated in colitis (Figure 9C,D). Compared with the DSS group, the expression of Nrf2 in the TRYP group was significantly increased, but the decrease of Keap1 in the TRYP and SASP group was not significant. The above results indicated that TRYP could further activate Nrf2 and produce antioxidant effects.

3. DISCUSSION

IN is a traditional Chinese medicine that has been used in clinical trials for thousand years. The main active ingredients in IN are indole alkaloids, including indirubin, indigo, and TRYP. It has been reported that indole compounds had notable anti-inflammatory effects and were a class of promising compounds.[30] Previous studies have shown that TRYP could inhibit the progression of inflammation, but its mechanism is still ambiguity. The purpose of this work was to explore the anti-inflammatory mechanism of TRYP through a combination of in vivo and in vitro experiments.

The balance of pro-inflammatory cytokines and anti-inflammatory cytokines plays important roles in the progression of UC. Our work demonstrated that TRYP could reduce the secretion and expression of pro-inflammatory factors, including IL-6, TNF-α, and NO in LPS-stimulated RAW264.7 cells. TMT proteomics technology is a method to predict the potential mechanism of pathophysiological processes by finding differentially expressed proteins.[31−33] A total of 12 proteins were obtained after TRYP treatment by the TMT proteomics technology. These proteins are predominantly distributed in the cell membrane and are involved in oxidoreductase activity, inflammatory responses, and cell phagocytosis. Further analysis showed that FcεRIγ, gp91phox, and p22phox interacted with each other.

FcεRI is a receptor for IgE, which exists in the human body as a trimer ($\alpha\gamma2$) and a tetramer ($\alpha\beta\gamma2$).[34] The aggregation of FcεRI could lead to the release of inflammatory mediators.[35] When cells are stimulated, Syk is recruited to ITAM and transmits downstream signals.[36] In LPS-stimulated RAW264.7 cells, MyD88 also activates Syk and the Syk-mediated NF-κB pathway and induces the Syk-mediated ROS production.[37] Moreover, MyD88 can activate IKK kinase, and IKK activation causes NF-κB to the nucleus and initiates a transcriptional program leading to expression of inflammatory targets.[38] We conducted western blot experiments, and the results demonstrated that FcεRIγ and *p*-SyK proteins were highly expressed post LPS stimulation in RAW264.7 cells compared to unstimulated macrophages. TRYP pretreatment significantly downregulated the expression of these two proteins. Molecular docking results demonstrated that TRYP could bind to FcεRIγ.

In the normal state of cells, NADPH oxidase is inactive as its components are distributed among the cytosol (p47phox, p67phox, p40phox, and Rac1/2), plasma membrane, and membranes of specific granules (p22phox and gp91phox).[39] When macrophages are externally stimulated, pathogens and pathogenic components are engulfed,[40] forming phagosomes in the cell, which fuse with lysosomes to form phagolysosomes. During this process, the cytoplasmic components of NADPH oxidase bind to the components of the cell membrane and assemble into oxidases with catalytic activity.[41,42] It is then transported to the phagosomal membrane during phagocytosis and releases superoxide radicals into the phagosome,[26] generating bactericidal ROS. Our proteomic results demonstrated that gp91phox and p22phox, the major component subunits of NADPH oxidase, were differentially expressed proteins, and the results of the later validation experiments also suggested that TRYP could significantly downregulate the high expression of gp91phox and p22phox proteins induced by LPS stimulation. Using molecular docking, we found that TRYP spontaneously binds to gp91 and p22phox.

Elevated levels of oxidative stress and sustained release of pro-inflammatory factors can threaten cell activity and growth. When excess ROS are generated, the cell starts to activate its antioxidant system to neutralize ROS and avoid damage.[43] The NADPH oxidase family is assumed to be the only group of ROS-producing enzymes, and the vast majority of ROS in the body is catalyzed by NADPH oxidases.[44,45] ROS can activate the NF-κB pathway by stimulating IKKα and IKKβ.[46] TRYP pretreatment is demonstrated to significantly reduce the elevation of ROS levels induced by arachidonic acid + iron.[47] Our results indicate that TRYP effectively inhibits LPS-induced intracellular ROS production. Thus, ROS is an important target for TRYP to inhibit the inflammatory response.

https://doi.org/10.1021/acsomega.4c03795
ACS Omega 2024, 9, 30904−30918

Table 2. Nucleotide Sequences of qRT-PCR Primers

gene name	forward primer sequence (5′−3′)	reverse primer sequence (5′−3′)
β-actin	GCTGTGCTATGTTGCTCTAG	CGCTCGTTGCCAATAGTG
IL-6	AGGATACCACTCCCAACAGACC	AAGTGCATCATCGTTGTTCATACA
TNF-α	CACGTCGTAGCAAACCACC	TGAGATCCATGCCGTTGGC

Oxidative stress is also directly related to intestinal inflammation during UC. The results showed that TRYP treatment could significantly reduce the content of MDA in the serum of UC mice and could restore the activity of antioxidant enzyme SOD. The Keap1/Nrf2 signaling pathway could reduce inflammation-induced damage by controlling oxidative stress. Activated Nrf2 is translocated to the nucleus and binds to ARE, thereby exerting an antioxidant damaging effect.[48−50] TRYP was previously reported to protect some cells from oxidative stress or inflammation through Nrf2 signaling, such as HaCaT cells,[51] BV2 microglia,[25] and HepG2 cells.[52] It was reported that TRYP may improve oxidative stress in psoriatic skin by increasing Nrf2 activation.[51] Our in vivo and in vitro results verified that TRYP pretreatment further activated Nrf2, promoted its entry into the nucleus, and initiated an antioxidant mechanism. Moreover, the activation of Nrf2 could also regulate the expression of intestinal tight junction proteins, thereby enhancing the integrity of the intestinal mucosal barrier and inhibiting the development of UC. Our work showed that TRYP treatment upregulated the expression of intestinal tight junction proteins ZO-1 and occludin in UC mice.

In the inflammatory response, the activation of the NF-κB signaling pathway is affected by a variety of cell signaling molecules, such as MyD88, ROS, Syk, IKKα/β, and IκB.[37] When TLR4 binds to its corresponding ligand, MyD88 attracts IRAK-4 to the TLRs, activating the IKK complex, which then activates NF-κB.[3] TRYP regulated inflammation by modulating the TLR4-MyD88 pathway.[53] Our results indicated that TRYP pretreatment could reduce the expression of TLR4 and MyD88 and inhibit the phosphorylation of IκBα, thereby suppressing the activation of NF-κB p65 into the nucleus. The results of the IF experiments confirmed this. These results indicated that TRYP produced a comparable effect to that of BAY 11−7082 (a NF-κB inhibitor). The results of our animal experiments also showed that TRYP treatment could inhibit the expression and nuclear translocation of NF-κB p65 in the colons of UC mice.

The activation of the TLR4-MyD88 can induce JAK phosphorylation, triggering STAT family activation.[54] The ROS signal also controls JAK, STAT3, and STAT5.[55] Upon ROS stimulation, STAT3 is activated through phosphorylation of the tyrosine 705 site (Tyr705) and translocates into the nucleus.[56] Studies have demonstrated that TRYP could inhibit IL-6 production in LPS-treated BV2 microglia and IL-6 secretion in colitis tissues.[23,25] IL-6 activates the JAK/STAT3 signaling pathway. Our in vitro studies demonstrated that TRYP inhibited p-STAT3 expression and translocation into the nucleus by inhibiting ROS and IL-6 production, which in turn regulated the JAK/STAT3 signaling pathway. Our in vivo studies also showed that TRYP treatment suppressed p-STAT3 expression and translocation into the nucleus in colonic tissues of UC mice.

4. MATERIALS AND METHODS

4.1. Materials. TRYP (LCMS Purity ≥99.89%, 46030) was from MedChemExpress (Monmouth Junction, NJ, USA). LPS (454420847) was from Sigma-Aldrich (St. Louis, MO, USA). BAY11−7082 (IκB/IKK inhibitor, 120920210531) was obtained from Beyotime Institute of Biotechnology (Shanghai, China). MTT was purchased from MP Biomedicals (Irvine, CA, USA). SPARKeasy Cell RNA Kit (DTNYF), SPARK script II RT Plus Kit (DMQQG), and 2× SYBR Green qPCR Mix (DTNLN) were purchased from Shandong Sikejie Biotechnology (Shandong, China). DSS (S0221) was purchased from MP Biomedicals (CA, USA). SASP tablets (22200301) were purchased from Shanghai Fuda Pharmaceutical Co., Ltd. (Shanghai, China). RIPA lysis buffer (17C16B17), DAPI (18C31C76), an antibody against β-actin (BST17353873), and histone H3 (BOS9110BP5687) were purchased from Boster Biological Technology (Wuhan, China). Rabbit monoclonal antibodies IκBα (4812S), phospho-IκBα (Ser32/36, 9246S), STAT3 (12640S), phospho-STAT3 (Tyr705, 9145T), JAK1 (3344S), JAK2 (3230S), phospho-JAK1 (Tyr1034/1035, 74129S), phospho-JAK2 (Tyr1007/1008, 3776S), NF-κB p65 (8242S), IKKβ (2678T), MyD88 (4283S), splenic tyrosine kinase (Syk) (13198T), phospho-Zap-70 (Try319)/Syk (Try352, 2717T), IKKα (2682S), Nrf2 (12721T), and Keap1 (8047S) were purchased from Cell Signaling Technology (Beverly, MA, USA). Antibodies against NOX2 (BBO1071023) were purchased from Bioss (Woburn, MA, USA). Anticytochrome b245 Light Chain/p22-phox (GR3400986-1) antibody was obtained from Abcam (Cambridge, MA, USA). Antibody against high affinity immunoglobulin epsilon receptor subunit γ (FcεRIγ) (0060020101) was purchased from Bio-Techne Corporation (Minneapolis, MN, USA).

4.2. Cells and Experimental Methods. *4.2.1. Cell Culture.* Mouse macrophages RAW264.7 cells (Shanghai Institute of Biological Sciences, Chinese Academy of Sciences (Shanghai, China)) were cultured in RPMI 1640 medium (with 1% streptomycin/penicillin and 10% FBS) at 37 °C with 5% CO_2,[57] in a constant temperature incubator.

4.2.2. Cell Viability Assay. RAW264.7 cells were inoculated in 96-well plates at 1.5×10^4 cells per well density. Post cell attachment, cells were treated with TRYP (0.025, 0.05, 0.25, 0.5, 1, 2.5, 5, 10, 15, 30, and 50 μg/mL) for 20 h. MTT solution (5 mg/mL) was incorporated and placed in an incubator for another 4 h; furthermore, DMSO was incorporated. Absorbance was measured at 450 nm.

4.2.3. NO, IL-6, and TNF-α Detection. RAW264.7 cells were seeded into 96-well plates at 2.5×10^5 cells per well density. Post cell attachment, cells were incorporated with TRYP (1, 2.5, 5 μg/mL) or BAY11−7082 (10 μM) for 1 h, and then the per well was treated with 1 μg/mL LPS for 24 h. The NO secretion was measured using the Griess method. IL-6 (M230112-004b) and TNF-α (M230403-102a) ELISA kits (Neobioscience Technology Company, Shenzhen, China) were used to determine their secretion levels.

https://doi.org/10.1021/acsomega.4c03795
ACS Omega 2024, 9, 30904−30918

4.2.4. RNA Extraction and qRT-PCR Analysis. RAW264.7 cells were cultured in 6-well plates at 2×10^6 cells/well density. Post cell apposition, the drug groups were treated as described in Section 2.4. Total RNA was obtained using a SPARKeasy Cell RNA Kit, and cDNA was obtained using a SPARK script II RT Plus Kit. A 2 × SYBR Green qPCR Mix was used, cDNA was added, and the target gene primer (Table 2) was incorporated for amplification. The specific parameters of the fluorescence quantification assay reaction procedure were as follows: 94 °C−94 °C−60 °C (3 min−10 s−30 s), fluorescence detection, repeated 2−3 steps for 40 cycles; solubility curves, measured Ct values for each group, and computed the relative expression of each gene.

4.2.5. Proteomics. 4.2.5.1. Protein Extraction and Peptide Enzymatic Digestion. The cell treatment method followed the protocol in Section 2.5. The samples were divided into control group and LPS and TRYP (2.5 μg/mL) groups. The methods of protein extraction and peptide enzymatic digestion were described in the previous literature.[58] Briefly, the lysate was added to extract the protein and quantified. After that, the proteins were trypsinized, desalted, and lyophilized. Finally, the peptides were quantified.

4.2.5.2. TMT Labeling and High pH Reverse Fractionation. The methods were described in the previous literature.[59] Briefly, each group of samples was labeled with a TMT labeling kit and fractionated with a high-pH reversed-phase peptide fractionation kit. Finally, desalination, gradient elution, drying, and finally using OD280 were used to determine the peptide concentration.

4.2.5.3. LC−MS/MS Instrument Detection Conditions. Chromatographic conditions: the specifications and methods of chromatographic columns and analytical columns were described in the previous literature.[60] The mass spectrometry conditions: scanning range of 300−1800 m/z. After each full scan, 20 fragment maps were collected.[61]

4.2.5.4. Bioinformatics Analysis. Proteomics data have been deposited with the ProteomeXchange Consortium (PXD050170). Some analysis software for hierarchical clustering analysis and protein subcellular localization were described in the previous literature.[62] Pfam database was used to evaluate protein structural domains. Domain annotation information for the target protein sequences was obtained by using the InterProScan software package. The software for GO and KEGG enrichment analysis of differential proteins was described in the previous literature.[63] The STRING database was used to look for correlations among differentially expressed proteins.

4.2.6. Immunofluorescence Assay. The cell treatment method followed the protocol in Section 2.5. The concentration of TRYP was 2.5 μg/mL. After cells were washed with PBS, 4% paraformaldehyde was incorporated for fixation. Next, 1% Triton (304L025; Solarbio Technology, Beijing, China) was incorporated and left to stand for 10 min. Five percent BSA (17L01A04; Boster Biological Technology, Wuhan, China) was incorporated and left to stand for 30 min. Diluted NF-κB p65 (1:1000), p-STAT3 (1:200), and Nrf2 antibody (1:2000) were incorporated into the wells. After that, the FITC-conjugated secondary antibody was added to the mixture for incubation. DAPI was incorporated for 5 min and observed using fluorescence microscopy.

4.2.7. ROS Level Detection. The cell treatment method was the same as in Section 2.5. The ROS content in each group was detected by using an ROS assay kit (101121220519; Beyotime, Shanghai, China). The cell culture medium in the 6-well plates was removed. The diluted dichlorodihydrofluorescein diacetate was added to the well. The results were observed by using a fluorescence microscope.

4.2.8. Western Blot Analysis. The cell treatment method followed the protocol in Section 2.5. Proteins were obtained using RIPA lysis buffer and a nuclear protein extraction kit (20230415; Solarbio Technology, Beijing, China). The proteins were first passed through gel electrophoresis, followed by membrane transfer. After the proteins were transferred to the PVDF membrane, the membrane was closed with a skimmed milk. The primary antibody was diluted with the primary antibody diluent (AR1017; Boster Biological Technology, Wuhan, China) at an appropriate ratio, and the PVDF membranes were incubated at 4 °C overnight. The PVDF membranes were placed in a TBST-diluted secondary antibody solution for 1 h. Superstar ECL Plus reagent (17K14B74; Boster Biological Technology, Wuhan, China) was incorporated into the PVDF membranes, which were then exposed using a gel imager.

4.2.9. Docking Analyses. Docking studies were conducted to understand the binding configuration of FcεRIγ (AF_P20491) or gp91phox (AF_Q61093) or p22phox (AF_Q61462) to TRYP using the AutoDock Vina program. The structure of TRYP was retrieved from PubChem database (https://pubchem.ncbi.nlm.nih.gov), while protein structures were obtained from AlphaFold protein structure database (https://alphafold.ebi.ac.uk/). A graphical interface (AutoDock Tools 1.5.6) was used to incorporate the polar hydrogen atoms into the protein. Molecular docking was conducted according to the standard procedures.

4.3. Animals and Experimental Methods. *4.3.1. Animals.* The purchase channels, feeding methods, feeding environment, modeling methods, and related ethics of the experimental animals were the same as those of our previous studies.[23] In our previous study, we have done the effects of three concentrations (39.2, 78.4, and 156.8 mg/kg) of TRYP on UC mice in a dose-dependent manner.[23] The effect of medium dose of 78.4 mg/kg was significant, so we used the medium dose of TRYP in this work. Briefly, forty C57BL/6 mice were randomly divided into a blank group (CON), model group (DSS), TRYP (78 mg/kg) group, and positive drug group (SASP, 125 mg/kg). UC mouse model was induced by freely drinking 2.5% DSS. All relevant animal procedures follow the relevant provisions of the Experimental Animal Ethics Committee of Shaanxi University of Traditional Chinese Medicine (ethical committee no. SUCMDL20230829001).

4.3.2. Observation of Pathological Changes of the Colon Tissue in Mice. The specific experimental methods of this part have been described in detail in our previous studies.[23] Briefly, after H&E staining of the colon, the pathological conditions of the colon tissues of the four groups were observed under a microscope.

4.3.3. Detection of MPO Activity in the Colon, and Levels of MDA and SOD in the Serum of Mice. Briefly, the MPO activity in the colon of the four groups of mice was detected by an MPO kit (20230913, NanJing JianCheng Bioengineering Institute, NanJing, China). The contents of MDA and SOD in the serum of four groups of mice were detected by MDA and SOD kits (20230913, 20231016, NanJing JianCheng Bioengineering Institute, NanJing, China).

https://doi.org/10.1021/acsomega.4c03795
ACS Omega 2024, 9, 30904−30918

4.3.4. Immunohistochemistry Assay. The specific experimental methods of this part have been described in detail in our previous studies.[23] Briefly, the mouse colon tissue samples were fixed, antigen repaired, blocking nonspecific binding, antibody binding, and finally closed for color observation.

4.3.5. Immunofluorescence Assay. The methods were described in the previous literature.[64] Briefly, the mouse colon tissue samples were fixed, antigen repaired, serum blocked, antibody binding, and DAPI staining of the nucleus, and finally sealed and observed.

4.4. Statistical Analysis. The experimental data were expressed as the mean ± SEM ($n \geq 3$). The statistical analysis and plotting were performed by using GraphPad Prism software (version 8.0). One-way ANOVA was used for comparisons among multiple groups. $^{\#}P < 0.05$ and $^{*}P < 0.05$ were considered statistically significant.

5. CONCLUSIONS

In this study, TRYP inhibited the TLR4/MyD88/ROS/NF-κB and JAK/STAT3 signaling pathways to exert anti-inflammatory effects. We preliminarily assumed that this effect may be attributed to the potential binding of TRYP to gp91phox, p22phox, and FcεRIγ proteins on the cell membrane. Additionally, TRYP exerts antioxidant effects by regulating the Keap1/Nrf2 signaling pathway. Therefore, TRYP should play a vital role in the clinical use of IN for the treatment of inflammation and may be a potential drug for the development of colitis treatment.

AUTHOR INFORMATION

Corresponding Authors

Yan-Ni Liang − *Co-construction Collaborative Innovation Center for Chinese Medicine Resources Industrialization by Shaanxi & Education Ministry, State Key Laboratory of Research & Development of Characteristic Qin Medicine Resources (Cultivation), Shaanxi University of Chinese Medicine, Xianyang 712083, China*; Email: aiziji_2005@126.com

Zheng Wang − *Co-construction Collaborative Innovation Center for Chinese Medicine Resources Industrialization by Shaanxi & Education Ministry, State Key Laboratory of Research & Development of Characteristic Qin Medicine Resources (Cultivation), Shaanxi University of Chinese Medicine, Xianyang 712083, China*; Email: wazh0405@126.com

Authors

Jie Zhu − *Co-construction Collaborative Innovation Center for Chinese Medicine Resources Industrialization by Shaanxi & Education Ministry, State Key Laboratory of Research & Development of Characteristic Qin Medicine Resources (Cultivation), Shaanxi University of Chinese Medicine, Xianyang 712083, China*; orcid.org/0000-0002-9768-2540

Wen Cheng − *Co-construction Collaborative Innovation Center for Chinese Medicine Resources Industrialization by Shaanxi & Education Ministry, State Key Laboratory of Research & Development of Characteristic Qin Medicine Resources (Cultivation), Shaanxi University of Chinese Medicine, Xianyang 712083, China*

Tian-Tian He − *Co-construction Collaborative Innovation Center for Chinese Medicine Resources Industrialization by Shaanxi & Education Ministry, State Key Laboratory of Research & Development of Characteristic Qin Medicine Resources (Cultivation), Shaanxi University of Chinese Medicine, Xianyang 712083, China*

Bao-Long Hou − *Co-construction Collaborative Innovation Center for Chinese Medicine Resources Industrialization by Shaanxi & Education Ministry, State Key Laboratory of Research & Development of Characteristic Qin Medicine Resources (Cultivation), Shaanxi University of Chinese Medicine, Xianyang 712083, China*

Li-Yan Lei − *Co-construction Collaborative Innovation Center for Chinese Medicine Resources Industrialization by Shaanxi & Education Ministry, State Key Laboratory of Research & Development of Characteristic Qin Medicine Resources (Cultivation), Shaanxi University of Chinese Medicine, Xianyang 712083, China*

Complete contact information is available at: https://pubs.acs.org/10.1021/acsomega.4c03795

Author Contributions

Methodology, J.Z., Y.N.L., and L.Y.L.; writing—original draft, J.Z.; visualization and validation, J.Z., W.C., and T.T.H.; writing—review and editing, J.Z., W.C., T.T.H., B.L.H., L.Y.L., Z.W., and Y.N.L.; and funding acquisition, B.L.H., Z.W., and Y.N.L.

Funding

This study was supported by the Key Research and Development Program of Shaanxi Province (2018ZDCXL-SF-01-02-02, 2022SF-222) and the Program for the National Natural Science Foundation of China (nos. 81803951, 82204235, and 81973687).

Notes

The animal ethics approval no. was SUCMDL20230829001 (29 Aug 2023) from the Experimental Animal Ethics Committee of Shaanxi University of Traditional Chinese Medicine.

The authors declare no competing financial interest.

ACKNOWLEDGMENTS

We would like to thank the Youth Innovation Team of Shaanxi Universities (Education Department of Shaanxi Provincial Government [2019], no. 90), the third batch of young outstanding talents support program in Shaanxi universities.

REFERENCES

(1) Tanaka, M.; Kishimoto, Y.; Sasaki, M.; Sato, A.; Kamiya, T.; Kondo, K.; Iida, K. Terminalia bellirica (Gaertn.) Roxb. Extract and Gallic Acid Attenuate LPS-Induced Inflammation and Oxidative Stress via MAPK/NF-κB and Akt/AMPK/Nrf2 Pathways. *Oxid. Med. Cell. Longevity* **2018**, *2018*, 1−15.

(2) Ren, J.; Su, D.; Li, L.; Cai, H.; Zhang, M.; Zhai, J.; Li, M.; Wu, X.; Hu, K. Anti-inflammatory effects of Aureusidin in LPS-stimulated RAW264.7 macrophages via suppressing NF-κB and activating ROS- and MAPKs-dependent Nrf2/HO-1 signaling pathways. *Toxicol. Appl. Pharmacol.* **2020**, *387*, 114846.

(3) Jiang, Z.; Shen, J.; Ding, J.; Yuan, Y.; Gao, L.; Yang, Z.; Zhao, X. USP18 mitigates lipopolysaccharide-induced oxidative stress and inflammation in human pulmonary microvascular endothelial cells through the TLR4/NF-κB/ROS signaling. *Toxicol. In Vitro* **2021**, *75*, 105181.

(4) Zhou, Y.; Wang, J.; Yang, W.; Qi, X.; Lan, L.; Luo, L.; Yin, Z. Bergapten prevents lipopolysaccharide-induced inflammation in RAW264.7 cells through suppressing JAK/STAT activation and ROS production and increases the survival rate of mice after LPS challenge. *Int. Immunopharmacol.* **2017**, *48*, 159−168.

(5) Lee, S. B.; Shin, J. S.; Han, H. S.; Lee, H. H.; Park, J. C.; Lee, K. T. Kaempferol 7- O - β -D-glucoside isolated from the leaves of Cudrania tricuspidata inhibits LPS-induced expression of pro-inflammatory mediators through inactivation of NF-κB, AP-1, and JAK-STAT in RAW 264.7 macrophages. *Chem.-Biol. Interact.* **2018**, *284*, 101−111.
(6) Dell'Albani, P.; Santangelo, R.; Torrisi, L.; Nicoletti, V. G.; de Vellis, J.; Giuffrida Stella, A. M. JAK/STAT signaling pathway mediates cytokine-induced iNOS expression in primary astroglial cell cultures. *J. Neurosci. Res.* **2001**, *65* (5), 417−424.
(7) Kim, H. Y.; Park, E. J.; Joe, E. H.; Jou, I. Curcumin suppresses Janus kinase-STAT inflammatory signaling through activation of Src homology 2 domain-containing tyrosine phosphatase 2 in brain microglia. *J. Immunol.* **2003**, *171* (11), 6072−6079.
(8) Kimura, A.; Naka, T.; Muta, T.; Takeuchi, O.; Akira, S.; Kawase, I.; Kishimoto, T. Suppressor of cytokine signaling-1 selectively inhibits LPS-induced IL-6 production by regulating JAK-STAT. *Proc. Natl. Acad. Sci. U.S.A.* **2005**, *102* (47), 17089−17094.
(9) Kou, X.; Qi, S.; Dai, W.; Luo, L.; Yin, Z. Arctigenin inhibits lipopolysaccharide-induced iNOS expression in RAW264.7 cells through suppressing JAK-STAT signal pathway. *Int. Immunopharmacol.* **2011**, *11* (8), 1095−1102.
(10) D'Amico, F.; Fasulo, E.; Jairath, V.; Paridaens, K.; Peyrin-Biroulet, L.; Danese, S. Management and treatment optimization of patients with mild to moderate ulcerative colitis. *Expert Rev. Clin. Immunol.* **2024**, *20* (3), 277−290.
(11) Hegarty, L. M.; Jones, G. R.; Bain, C. C. Macrophages in intestinal homeostasis and inflammatory bowel disease. *Nat. Rev. Gastroenterol. Hepatol.* **2023**, *20* (8), 538−553.
(12) Le Berre, C.; Honap, S.; Peyrin-Biroulet, L. Ulcerative colitis. *Lancet* **2023**, *402* (10401), 571−584.
(13) Xiong, L.; Dean, J. W.; Fu, Z.; Oliff, K. N.; Bostick, J. W.; Ye, J.; Chen, Z. E.; Mühlbauer, M.; Zhou, L. Ahr-Foxp3-RORγt axis controls gut homing of CD4(+) T cells by regulating GPR15. *Sci. Immunol.* **2020**, *5* (48), No. eaaz7277.
(14) Xu, X.-R.; Tang, J.-F.; Zhang, H.; Ran, F.; Liao, W.; Wang, F.; Yang, X. B.; Lin, J. Z.; Yang, M.; Zhang, D. K.; Han, L. [Antipyretic activity and potential mechanism of Indigo Naturalis on 2,4-dinitrophenol-induced fever rat model]. *Zhongguo Zhongyao Zazhi* **2021**, *46* (13), 3205−3212.
(15) Yang, X.; Tang, J.; Su, J.; Yang, X.; Yang, M.; Yang, X.; Ji, Q.; He, Y.; Han, L.; Zhang, D. High-Quality Indigo Naturalis Obtained with Automatic Foam Separation. *ACS Appl. Mater. Interfaces* **2023**, *15* (37), 43272−43281.
(16) Naganuma, M. Treatment with indigo naturalis for inflammatory bowel disease and other immune diseases. *Immunol. Med.* **2019**, *42* (1), 16−21.
(17) Saiki, J. P.; Andreasson, J. O.; Grimes, K. V.; Frumkin, L. R.; Sanjines, E.; Davidson, M. G.; Park, K. T.; Limketkai, B. Treatment-refractory ulcerative colitis responsive to indigo naturalis. *BMJ Open Gastroenterol.* **2021**, *8* (1), No. e000813.
(18) Li, R.; Xue, C.; Pan, Y.; Li, G.; Huang, Z.; Xu, J.; Zhang, J.; Chen, X.; Hou, L. Research on different compound combinations of Realgar-Indigo naturalis formula to reverse acute promyelocytic leukemia arsenic resistance by regulating autophagy through mTOR pathway. *J. Ethnopharmacol.* **2024**, *326*, 117778.
(19) Zhang, Q.; Xie, J.; Li, G.; Wang, F.; Lin, J.; Yang, M.; Du, A.; Zhang, D.; Han, L. Psoriasis treatment using Indigo Naturalis: Progress and strategy. *J. Ethnopharmacol.* **2022**, *297*, 115522.
(20) Xie, J.; Huang, Q.; Xie, H.; Liu, J.; Tian, S.; Cao, R.; Yang, M.; Lin, J.; Han, L.; Zhang, D. Hyaluronic acid/inulin-based nanocrystals with an optimized ratio of indigo and indirubin for combined ulcerative colitis therapy via immune and intestinal flora regulation. *Int. J. Biol. Macromol.* **2023**, *252*, 126502.
(21) Sun, S.; Lv, B. The antiferroptotic effect of indigo on ulcerative colitis. *J. Gastroenterol.* **2024**, *59* (1), 75−76.
(22) Han, N. R.; Moon, P. D.; Kim, H. M.; Jeong, H. J. Tryptanthrin ameliorates atopic dermatitis through down-regulation of TSLP. *Arch. Biochem. Biophys.* **2014**, *542*, 14−20.
(23) Wang, Z.; Wu, X.; Wang, C. L.; Wang, L.; Sun, C.; Zhang, D. B.; Liu, J. L.; Liang, Y. N.; Tang, D. X.; Tang, Z. S. Tryptanthrin Protects Mice against Dextran Sulfate Sodium-Induced Colitis through Inhibition of TNF-α/NF-κB and IL-6/STAT3 Pathways. *Molecules* **2018**, *23* (5), 1062.
(24) Zhu, J.; Hou, B. L.; Cheng, W.; Wang, T.; Wang, Z.; Liang, Y. N. [Mechanism of tryptanthrin in treatment of ulcerative colitis in mice based on serum metabolomics]. *Zhongguo Zhongyao Zazhi* **2023**, *48* (8), 2193−2202.
(25) Kwon, Y. W.; Cheon, S. Y.; Park, S. Y.; Song, J.; Lee, J. H. Tryptanthrin Suppresses the Activation of the LPS-Treated BV2Microglial Cell Line via Nrf2/HO-1 Antioxidant Signaling. *Front. Cell. Neurosci.* **2017**, *11*, 18.
(26) Rada, B.; Leto, T. L. Oxidative innate immune defenses by Nox/Duox family NADPH oxidases. *Contrib. Microbiol.* **2008**, *15*, 164−187.
(27) Travers, T.; Kanagy, W. K.; Mansbach, R. A.; Jhamba, E.; Cleyrat, C.; Goldstein, B.; Lidke, D. S.; Wilson, B. S.; Gnanakaran, S. Combinatorial diversity of Syk recruitment driven by its multivalent engagement with FcεRIγ. *Mol. Biol. Cell* **2019**, *30* (17), 2331−2347.
(28) Wright, J. G.; Christman, J. W. The role of nuclear factor kappa B in the pathogenesis of pulmonary diseases: implications for therapy. *Am. J. Respir. Med.* **2003**, *2* (3), 211−219.
(29) Yu, C.; Xiao, J. H. The Keap1-Nrf2 System: A Mediator between Oxidative Stress and Aging. *Oxid. Med. Cell. Longevity* **2021**, *2021*, 1−16.
(30) Cho, B.; Yoon, S. M.; Son, S. M.; Kim, H. W.; Kim, K. B.; Youn, S. J. Ischemic colitis induced by indigo naturalis in a patient with ulcerative colitis: a case report. *BMC Gastroenterol.* **2020**, *20* (1), 154.
(31) Birnbaumer, L.; Yidirim, E.; Abramowitz, J. A comparison of the genes coding for canonical TRP channels and their M, V and P relatives. *Cell Calcium* **2003**, *33* (5−6), 419−432.
(32) McGarvey, L. P.; Butler, C. A.; Stokesberry, S.; Polley, L.; McQuaid, S.; Abdullah, H.; Ashraf, S.; McGahon, M. K.; Curtis, T. M.; Arron, J.; Choy, D.; Warke, T. J.; Bradding, P.; Ennis, M.; Zholos, A.; Costello, R. W.; Heaney, L. G. Increased expression of bronchial epithelial transient receptor potential vanilloid 1 channels in patients with severe asthma. *J. Allergy Clin. Immunol.* **2014**, *133* (3), 704−712.e4.
(33) De Logu, F.; Patacchini, R.; Fontana, G.; Geppetti, P. TRP functions in the broncho-pulmonary system. *Semin. Immunopathol.* **2016**, *38* (3), 321−329.
(34) Qiao, Y.; Chen, J. Investigating the inflammatory cascade effect of basophil activation in children with allergic rhinitis or asthma, via the IgE-FcεRI-NF-κB signaling pathway. *J. Allergy Clin. Immunol.* **2021**, *30* (7), 673−679.
(35) Kimura, T.; Kihara, H.; Bhattacharyya, S.; Sakamoto, H.; Appella, E.; Siraganian, R. P. Downstream signaling molecules bind to different phosphorylated immunoreceptor tyrosine-based activation motif (ITAM) peptides of the high affinity IgE receptor. *J. Biol. Chem.* **1996**, *271* (44), 27962−27968.
(36) Lin, K. C.; Huang, D. Y.; Huang, D. W.; Tzeng, S. J.; Lin, W. W. Inhibition of AMPK through Lyn-Syk-Akt enhances FcεRI signal pathways for allergic response. *J. Mol. Med.* **2016**, *94* (2), 183−194.
(37) Yi, Y. S.; Kim, H. G.; Kim, J. H.; Yang, W. S.; Kim, E.; Jeong, D.; Park, J. G.; Aziz, N.; Kim, S.; Parameswaran, N.; Cho, J. Y. Syk-MyD88 Axis Is a Critical Determinant of Inflammatory-Response in Activated Macrophages. *Front. Immunol.* **2021**, *12*, 767366.
(38) Miller, Y. I.; Choi, S. H.; Wiesner, P.; Bae, Y. S. The SYK side of TLR4: signalling mechanisms in response to LPS and minimally oxidized LDL. *Br. J. Pharmacol.* **2012**, *167* (5), 990−999.
(39) El-Benna, J.; Dang, P. M.; Périanin, A. Peptide-based inhibitors of the phagocyte NADPH oxidase. *Biochem. Pharmacol.* **2010**, *80* (6), 778−785.
(40) Honey, K.; Rudensky, A. Y. Lysosomal cysteine proteases regulate antigen presentation. *Nat. Rev. Immunol.* **2003**, *3* (6), 472−482.

https://doi.org/10.1021/acsomega.4c03795
ACS Omega 2024, 9, 30904−30918

(41) Cooney, S. J.; Bermudez-Sabogal, S. L.; Byrnes, K. R. Cellular and temporal expression of NADPH oxidase (NOX) isotypes after brain injury. *J. Neuroinflammation* **2013**, *10*, 917.
(42) Sul, O. J.; Ra, S. W. Quercetin Prevents LPS-Induced Oxidative Stress and Inflammation by Modulating NOX2/ROS/NF-kB in Lung Epithelial Cells. *Molecules* **2021**, *26* (22), 6949.
(43) Fan, Y.; Mao, R.; Yang, J. NF-κB and STAT3 signaling pathways collaboratively link inflammation to cancer. *Protein Cell* **2013**, *4* (3), 176−185.
(44) Mittal, M.; Siddiqui, M. R.; Tran, K.; Reddy, S. P.; Malik, A. B. Reactive oxygen species in inflammation and tissue injury. *Antioxid. Redox Signaling* **2014**, *20* (7), 1126−1167.
(45) Petry, A.; Görlach, A. Regulation of NADPH Oxidases by G Protein-Coupled Receptors. *Antioxid. Redox Signaling* **2019**, *30* (1), 74−94.
(46) Kamata, H.; Manabe, T.; Oka, S.; Kamata, K.; Hirata, H. Hydrogen peroxide activates IκB kinases through phosphorylation of serine residues in the activation loops. *FEBS Lett.* **2002**, *519* (1−3), 231−237.
(47) Jung, E. H.; Jung, J. Y.; Ko, H. L.; Kim, J. K.; Park, S. M.; Jung, D. H.; Park, C. A.; Kim, Y. W.; Ku, S. K.; Cho, I. J.; Kim, S. C. Tryptanthrin prevents oxidative stress-mediated apoptosis through AMP-activated protein kinase-dependent p38 mitogen-activated protein kinase activation. *Arch. Pharmacal Res.* **2017**, *40* (9), 1071−1086.
(48) McMahon, M.; Lamont, D. J.; Beattie, K. A.; Hayes, J. D. Keap1 perceives stress via three sensors for the endogenous signaling molecules nitric oxide, zinc, and alkenals. *Proc. Natl. Acad. Sci. U.S.A.* **2010**, *107* (44), 18838−18843.
(49) Gong, Q.; Xue, Y.; Li, X.; Song, L.; Zhu, L. DL-3-n-butylphthalide attenuates lipopolysaccharide-induced acute lung injury via SIRT1-dependent and -independent regulation of Nrf2. *Int. Immunopharmacol.* **2019**, *74*, 105658.
(50) Ye, J.; Guan, M.; Lu, Y.; Zhang, D.; Li, C.; Zhou, C. Arbutin attenuates LPS-induced lung injury via Sirt1/ Nrf2/ NF-κBp65 pathway. *Pulm. Pharmacol. Ther.* **2019**, *54*, 53−59.
(51) Xiong, Y.; Wang, J.; Wang, S.; Li, H.; Zhou, X. Tryptanthrin ameliorates imiquimod-induced psoriasis in mice by suppressing inflammation and oxidative stress via NF-κB/MAPK/Nrf2 pathways. *J. Nat. Med.* **2023**, *77* (1), 188−201.
(52) Moon, S. Y.; Lee, J. H.; Choi, H. Y.; Cho, I. J.; Kim, S. C.; Kim, Y. W. Tryptanthrin protects hepatocytes against oxidative stress via activation of the extracellular signal-regulated kinase/NF-E2-related factor 2 pathway. *Biol. Pharm. Bull.* **2014**, *37* (10), 1633−1640.
(53) Shabna, A.; Antony, J.; Vijayakurup, V.; Saikia, M.; Liju, V. B.; Retnakumari, A. P.; Amrutha, N. A.; Alex, V. V.; Swetha, M.; Aiswarya, S. U.; Jannet, S.; Unni, U. S.; Sundaram, S.; Sherin, D. R.; Anto, N. P.; Bava, S. V.; Chittalakkottu, S.; Ran, S.; Anto, R. J. Pharmacological attenuation of melanoma by tryptanthrin pertains to the suppression of MITF-M through MEK/ERK signaling axis. *Cell. Mol. Life Sci.* **2022**, *79* (9), 478.
(54) Pizzino, G.; Irrera, N.; Cucinotta, M.; Pallio, G.; Mannino, F.; Arcoraci, V.; Squadrito, F.; Altavilla, D.; Bitto, A. Oxidative Stress: Harms and Benefits for Human Health. *Oxid. Med. Cell. Longevity* **2017**, *2017*, 1−13.
(55) Krylatov, A. V.; Maslov, L. N.; Voronkov, N. S.; Boshchenko, A. A.; Popov, S. V.; Gomez, L.; Wang, H.; Jaggi, A. S.; Downey, J. M. Reactive Oxygen Species as Intracellular Signaling Molecules in the Cardiovascular System. *Curr. Cardiol. Rev.* **2018**, *14* (4), 290−300.
(56) Xu, F.; Xu, J.; Xiong, X.; Deng, Y. Salidroside inhibits MAPK, NF-κB, and STAT3 pathways in psoriasis-associated oxidative stress via SIRT1 activation. *Redox Rep.* **2019**, *24* (1), 70−74.
(57) Liu, Y.; Tian, S.; Yi, B.; Feng, Z.; Chu, T.; Liu, J.; Zhang, C.; Zhang, S.; Wang, Y. Platycodin D sensitizes KRAS-mutant colorectal cancer cells to cetuximab by inhibiting the PI3K/Akt signaling pathway. *Front. Oncol.* **2022**, *12*, 1046143.
(58) Huo, B.; Song, Y.; Tan, B.; Li, J.; Zhang, J.; Zhang, F.; Chang, L. TMT-based proteomics analysis of the effects of Qianjinweijing Tang on lung cancer. *Biomed. Chromatogr.* **2021**, *35* (8), No. e5116.
(59) Li, X.; Wang, Q.; Wang, M.; Wuhan, B.; Gu, Y.; Kang, T.; Jin, H.; Xu, J. TMT-based quantitative proteomic analysis reveals the underlying mechanisms of glycidyl methacrylate-induced 16HBE cell malignant transformation. *Toxicology* **2023**, *485*, 153427.
(60) Liu, L.; Li, H.; Li, N.; Li, S.; Guo, J.; Li, X. Parental salt priming improves the low temperature tolerance in wheat offspring via modulating the seed proteome. *Plant Sci.* **2022**, *324*, 111428.
(61) Chen, Y.; Zhou, B.; Li, J.; Tang, H.; Zeng, L.; Chen, Q.; Cui, Y.; Liu, J.; Tang, J. Effects of Long-Term Non-Pruning on Main Quality Constituents in 'Dancong' Tea (Camellia sinensis) Leaves Based on Proteomics and Metabolomics Analysis. *Foods* **2021**, *10* (11), 2649.
(62) Zhu, R.; Chen, S. Proteomic analysis reveals semaglutide impacts lipogenic protein expression in epididymal adipose tissue of obese mice. *Front. Endocrinol.* **2023**, *14*, 1095432.
(63) Cheng, Y.; Wang, G.; Zhao, L.; Dai, S.; Han, J.; Hu, X.; Zhou, C.; Wang, F.; Ma, H.; Li, B.; Meng, Z. Periplocymarin Induced Colorectal Cancer Cells Apoptosis Via Impairing PI3K/AKT Pathway. *Front. Oncol.* **2021**, *11*, 753598.
(64) Zhou, M.; Ma, X.; Gao, M.; Wu, H.; Liu, Y.; Shi, X.; Dai, M. Paeonol Attenuates Atherosclerosis by Inhibiting Vascular Smooth Muscle Cells Senescence via SIRT1/P53/TRF2 Signaling Pathway. *Molecules* **2024**, *29* (1), 261.

https://doi.org/10.1021/acsomega.4c03795
ACS Omega 2024, 9, 30904−30918